The RNA-Splicing Ligase RTCB Promotes Influenza A Virus Replication by Suppressing Innate Immunity via Interaction with RNA Helicase DDX1

Lei Cao,*,† Xianfeng Hui,*,† Ting Xu,*,† Haiying Mao,*,† Xian Lin,*,† Kun Huang,*,† Lianzhong Zhao,‡,1 and Meilin Jin*,†,§,¶,1

The RNA-splicing ligase RNA 2′,3′-cyclic phosphate and 5′-OH ligase (RTCB) is a catalytic subunit of the tRNA-splicing ligase complex, which plays an essential role in catalyzing tRNA splicing and modulating the unfolded protein response. However, the function of RTCB in influenza A virus (IAV) replication has not yet been described. In this study, RTCB was revealed to be an IAV-suppressed host factor that was significantly downregulated during influenza virus infection in several transformed cell lines, as well as in primary human type II alveolar epithelial cells, and its knockout impaired the propagation of the IAV. Mechanistically, RTCB depletion led to a robust elevation in the levels of type I and type III IFNs and proinflammatory cytokines in response to IAV infection, which was confirmed by RTCB overexpression studies. Lastly, RTCB was found to compete with DDX21 for RNA helicase DDX1 binding, attenuating the DDX21-DDX1 association and thus suppressing the expression of IFN and downstream IFN-stimulated genes. Our study indicates that RTCB plays a critical role in facilitating IAV replication and reveals that the RTCB-DDX1 binding interaction is an important innate immunomodulator for the host to counteract viral infection. ***The Journal of Immunology*****, 2023, 211: 1020–1031.**

Influenza A virus (IAV) is an important human respiratory pathogen that circulates in multiple hosts and poses a recurrent threat to human health worldwide (1, 2). IAV belongs to the Orthomyxoviridae family and possesses eight segmented and single-stranded genomic RNAs (3). During IAV infection, viral RNAs are recognized and bound by host pattern recognition receptors such as TLR7 and RIG-I (also known as DDX58), which in turn elicit type I IFNs and proinflammatory responses to limit IAV infection (4, 5). The initiated innate immune responses are crucial for the subsequent viral clearance and the development of infection resistance. During the infection process, the level of immunological response should be strictly modulated to suppress infection and avoid potential immunotoxicity caused by cytokine storms (6, 7). Given that a balanced and moderate activation of the innate immune response is critical for host protective defense, an in-depth understanding of the fundamental mechanisms orchestrating innate immune responses during IAV infection would greatly aid in the development of effective antiviral approaches.

Type I IFN boost is considered the most important and powerful innate immune response to restrict viral infection, which can be modulated by either the host factors or the viral components (8, 9). An array of pattern recognition receptors in the human host, such as TLRs, retinoic acid–inducible gene I (RIG-I)-like helicases, and nucleotide-binding domain and leucine-rich repeat-containing proteins, are responsible for sensing pathogen-associated molecular patterns including viral materials (10). Previously, the DDX1-DDX21-DHX36 complex has been shown to play a crucial role in sensing dsRNA and activating the IFN responses (11, 12). Upon viral or dsRNA-like polycytidine-polycytidylic acid [poly(IC)] stimulation, the RNA helicase DDX1 binds to poly(IC), whereas DDX21 and DHX36 bind to the cytosolic Toll/IL-1R domain of the TRIF protein, leading to the activation of downstream immune responses. A recently published observation discovered that caspase-dependent cleavage of the DDX21 RNA helicase inhibited its association with DDX21 and DHX36, thereby compromising host innate immunity (13). However, IAV has evolved to evade the host's innate immune response through complicated mechanisms (14). For example, the NS1 protein of IAV antagonizes host defense mechanisms by inhibiting the ubiquitin ligase activity of TRIM25 and disrupting the formation of host antiviral components called stress granules (15, 16). Interestingly, our previous study revealed that influenza A M2 protein promoted host innate immunity by antagonizing the autophagy pathway and increasing mitochondrial antiviral signaling protein aggregation (17, 18). Chen et al. (19) showed that DDX21-PB1 interaction led to a

*State Key Laboratory of Agricultural Microbiology, Huazhong Agricultural University, Wuhan, China; †College of Animal Medicine, Huazhong Agricultural University, Wuhan, China; ‡College of Life Sciences and Oceanography, Shenzhen University, Shenzhen, China; §China Key Laboratory of Development of Veterinary Diagnostic Products, Ministry of Agriculture, Wuhan, China; and ¶The Cooperative Innovation Center for Sustainable Pig Production, Wuhan, China

[1]L.Z. and M.J. contributed equally to this work.

ORCID: 0000-0003-4332-4083 (M.J.).

Received for publication October 31, 2022. Accepted for publication July 11, 2023.

This work was supported by the National Natural Science Foundation of China (31820103015).

L.C., L.Z., and M.J. conceived and designed the experiments. L.C., X.H., and T.X. performed the experiments. M.J. and L.Z. analyzed the data. H.M., X.L., and K.H. contributed to the reagents and materials. L.Z. and M.J. wrote the paper. All authors contributed to the article and approved the submitted version.

Address correspondence and reprint requests to Prof. Meilin Jin or Dr. Lianzhong Zhao, Huazhong Agricultural University, No. 1, Shizishan Street, Hongshan District, Wuhan, Hubei Province 430070, P.R. China (M.J.) or Shenzhen University, No. 1066, Xueyuan Road, Nanshan District, Shenzhen 518060, P.R. China (L.Z.). E-mail addresses: jinmeilin@mail.hzau.edu.cn (M.J.) or lianzhongzhao@szu.edu.cn (L.Z.)

The online version of this article contains supplemental material.

Abbreviations used in this article: Cat no., catalog number; CCK-8, cell counting kit-8; co-IP, coimmunoprecipitation; HDV, hepatitis δ virus; H1N1-PR8, influenza A/Puerto Rico/8/34; H3N2-HB, strain A/Hunan/Hubei/3/2005; H5N6-JX, IAV strain A/duck/Hubei/WH18/2015; hpi, hours postinfection; IAV, influenza A virus; IOD, integrated OD; IRF, IFN regulatory factor; ISG, IFN-stimulated gene; ISRE, IFN-sensitive responsive element; KO, knockout; MOI, multiplicity of infection; poly(IC), polycytidine-polycytidylic acid; qPCR, quantitative PCR; RIG-I, retinoic acid–inducible gene I; RTCB, RNA 2′,3′-cyclic phosphate and 5′-OH ligase; RT-qPCR, reverse transcription-quantitative PCR; SeV, Sendai virus; sgRNA, single guide RNA; SINV, sindbis virus; siRNA, small interfering RNA; vRNP, viral ribonucleoprotein; VSV, vesicular stomatitis virus; WT, wild-type.

reduced polymerase assembly, which could be further reversed by the DDX21-NS1 association. The DDX1-DDX21-DHX36 complex appears to be particularly vulnerable to viral infection, and whether this complex could be disrupted by any other factors is yet to be fully elucidated.

RNA-splicing ligase (RNA 2′,3′-cyclic phosphate and 5′-OH ligase [RTCB], also termed HSPC1170) is involved in many cellular life processes, including tRNA splicing (20, 21), RNA repair (22), RNA recombination (23), and unfolded protein response in eukaryotes, bacteria, and archaea (24, 25). As an essential catalytic subunit of the tRNA ligase complex, RTCB is incorporated with DDX1 and FAM98A to perform multiple RNA ligation pathways. Moreover, an RNA interference screen revealed that RTCB could promote human hepatitis δ virus RNA accumulation in HEK293 cells (26). In sindbis virus (SINV) infection, RTCB has been identified as a viral RNA-binding protein, and its tRNA ligase complex positively contributes to SINV replication (27). In one of our previous studies, we identified RTCB as a protein component in the IAV viral ribonucleoprotein (vRNP) complex, consistent with the reports from other research groups (28, 29). Moreover, a recent study has revealed that RTCB interacts with IAV NS1 protein and may play a role in host defense and immune signaling pathways (30). These findings indicate a potential role of RTCB in IAV infection; however, a more detailed investigation is required.

In this study, we showed that RTCB expression in A549 cells decreased after infection with various subtypes of the influenza virus, which was reproduced in THP1, U251, and HEK293T cell lines and primary human type II alveolar epithelial cells. Furthermore, IAV replication was severely restricted by RTCB depletion. Mechanistically, depletion of RTCB favored the production of type I and type III IFNs during IAV infection, whereas overexpression of RTCB exhibited the opposite effect. In addition, RTCB appeared to compete with DDX21 for RNA helicase DDX1 binding, resulting in attenuated DDX21-DDX1 association, which suppressed the expression of IFN and its downstream antiviral genes.

Materials and Methods

Cells and viruses

A549 cells were cultured in Ham's F-12 medium (HyClone, Beijing, China). HEK293T, U251, and MDCK cells were cultured in DMEM (HyClone). THP-1 cells were cultured in RPMI 1640 basic medium (HyClone). All these transformed cell lines were sourced from the American Type Culture Collection (Manassas, VA). The primary human type II alveolar epithelial cells were provided by Pricella (Wuhan, China) and were cultured in human type II alveolar epithelial cells specific complete culture medium (Pricella). All basic culture media were supplemented with 10% FBS (PAN-Biotech, Aidenbach, Germany) and 1% penicillin-streptomycin. All cells were cultured at 37°C in 5% CO_2. The IAV strain A/duck/Hubei/WH18/2015 (H5N6-JX) (GenBank accession number KX652135, https://www.ncbi.nlm.nih.gov/nuccore/KX652135.1) and strain A/Hunan/Hubei/3/2005 (H3N2-HB) were isolated from duck and human, respectively. Influenza A/Puerto Rico/8/34 (H1N1-PR8) was conserved in our laboratory. H5N6-GFP recombinant virus was constructed based on the wild-type (WT) H5N6-JX strain. Vesicular stomatitis virus (VSV)-GFP and Sendai virus (SeV) were kindly provided by the Harbin Veterinary Research Institute (Harbin, China) and Prof. Z. Jiang (Peking University, Beijing, China).

Virus manipulation

After reaching 80% confluence, the cells were washed with PBS twice, followed by incubation with the diluted viruses for 1 h at 37°C in 5% CO_2. The viral diluent was removed and replaced with a medium containing 1% penicillin-streptomycin without FBS. The influenza viruses were manipulated in a biosafety level 3 laboratory administered by Huazhong Agricultural University. All experimental procedures were approved by the Institutional Biosafety Committee of Huazhong Agricultural University.

Plasmids and RNA compounds

The RNA of A549 cells was extracted and reverse transcribed into cDNA, which was subsequently used for RTCB, DDX1, DDX21, and DHX36 amplification. The RTCB and DHX36 genes was inserted into the eukaryotic expression vector pcDNA3.1-Myc, and the final recombinant vector was referred to as Myc-RTCB and Myc-DHX36. The DDX1 and DDX21 genes were cloned into the pCGGS-HA and pCMV-3xFlag plasmids and designated as HA-DDX1 and DDX21-Flag, respectively. Poly(IC) was commercially sourced from Sigma-Aldrich (St. Louis, MO; catalog number [Cat no.] 42424-50-0). Small interfering RNAs (siRNAs) targeting RTCB and DDX1 were purchased from Tsingke (Beijing, China). Knockdown efficiency was determined via Western blotting and quantitative PCR (qPCR).

Abs

The Abs used in this study were anti-RTCB rabbit polyclonal Ab (Cat no. 19809-1-AP; Proteintech), anti-DDX1 rabbit polyclonal Ab (Cat no. 11357-1-AP; Proteintech), anti-DDX21 rabbit polyclonal Ab (Cat no. 10528-1-AP; Proteintech), anti-DHX36 rabbit polyclonal Ab (Cat no. 13159-1-AP; Proteintech), anti-Flag mouse mAb (Cat no. F1804; Sigma), anti-HA rabbit polyclonal Ab (Cat no. 51064-2-AP; Proteintech), anti-GAPDH mouse mAb (Cat no. 60004-1-Ig; Proteintech), as well as Alexa Fluor 488–conjugated AffiniPure goat anti-mouse (Cat no. GM200G-02C; Sungene Biotech, Tianjin, China) and Alexa Fluor 594–conjugated AffiniPure goat anti-rabbit (Cat no. GR200G-43C; Sungene Biotech) secondary Abs.

Generation of the RTCB knockout cells

RTCB knockout (KO; $RTCB^{KO}$) A549, THP1, and U251 cells were generated by using the CRISPR/Cas9 system as described previously (31). Two single guide RNAs (sgRNAs) targeting the human RTCB gene (sgRTCB, $RTCB^{KO}$) and a control sgRNA targeting the luciferase gene (sgLuc, $RTCB^{WT}$) were cloned into the lentiCRISPR v2 vector, which was used for cotransfection with psPAX2 and pMD2G to produce recombinant lentiviruses. The A549, THP1, and U251 Cas9-expressing cells were transduced with the sgRTCB or sgLuc lentiviruses. At 48 h postinfection (hpi), the cells were subjected to puromycin selection (2.5 μg/ml) to obtain pooled $RTCB^{KO}$ or control clones.

Generation of the stable RTCB-overexpressing cell lines

Myc-tagged RTCB was cloned into the pCDH-CMV vector, which was used for cotransfection with psPAX2 and pMD2G to produce a recombinant lentivirus. The A549, THP1, and U251 cells were transduced with the Myc-RTCB lentiviruses. At 48 hpi, the cells were subjected to puromycin selection (2.5 μg/ml) to obtain pooled RTCB-expressing clones.

Viral plaque assay

MDCK cells (1.0×10^6/ml) were inoculated in six-well plates. When the cells covered 100% of the well, they were infected with 10-fold-diluted cell supernatants as described earlier for 1 h. After aspirating the diluted virus, the cells were cultured in 3 ml 2× MEM containing 2% agar (Sigma-Aldrich, MO) and 2 mg/ml tosylsulfonyl phenylalanyl chloromethyl ketone (Sigma-Aldrich) at 37°C in 5% CO_2 for 48–72 h. Finally, the plaque numbers were obtained through counting after crystal violet staining (Sigma-Aldrich).

Quantitative RT-PCR assay

Total cellular RNA was extracted from cells using the TRIzol reagent (Invitrogen) according to the manufacturer's instructions. The RNA was treated with DNase before being used to generate cDNA with reverse transcriptase (AMV XL; TaKaRa, Tokyo, Japan). The cDNA was then used as the template in an SYBR Green-based RT-PCR, which was performed on the ABI QuantStudio 6 PCR system (Applied Biosystems). The sequences of all primers and siRNAs used in this study are available from the corresponding author upon request.

Fluorescence and indirect immunofluorescence imaging

For fluorescence imaging, $RTCB^{WT}$ and two sgRNA-directed $RTCB^{KO}$ A549 cells were infected with H5N6-GFP (multiplicity of infection [MOI] = 0.01) or VSV-GFP (MOI = 0.01) viruses. At 24 hpi, the cells were fixed with 4% paraformaldehyde and then were permeabilized with 0.3% (v/v) Triton X-100 prepared in PBS, followed by nucleus staining with Hoechst (blue). Fluorescence images (GFP and Hoechst) were taken by immunofluorescence microscopy (EVOS FL Auto; ThermoFisher). For indirect immunofluorescence imaging, HeLa cells were grown on coverslips and transfected with HA-DDX1 and/or Myc-RTCB. Then the transfected cells were washed twice with PBS and fixed with 4% paraformaldehyde for 15 min, permeabilized using 0.2% (v/v) Triton X-100 for 15 min, and blocked with 1% (v/w) BSA for 30 min. Coverslips were incubated with primary Abs for 2 h and then with the appropriate Alexa Fluor–conjugated secondary Ab for 1 h before the nuclei

were stained with DAPI (Cat no. C1002; Beyotime, Jiangsu, China) for 15 min at room temperature. The stained samples were observed using a confocal microscope (LSM 880; Zeiss, Oberkochen, Germany). All experiments were repeated at least three times, and a representative result was shown.

Western blotting

Cells were lysed in Western and IP Cell lysis buffer (Beyotime, Shanghai, China) after two PBS washes. Proteins were quantified by standardization. Each protein sample was separated using 10–12% SDS-PAGE and transferred onto a polyvinylidene difluoride membrane. Subsequently, the membrane was immersed in 5% milk for 1 h at ambient temperatures and incubated with primary and secondary Abs successively. Finally, images were captured using an ECL detection system (Tannon, Beijing, China). The integrated OD (IOD) of RTCB and GAPDH blots was determined using Image-Pro Plus software (Media Cybernetics, Rockville, MD), and the relative IOD of RTCB was calculated by IOD RTCB/IOD GAPDH. All the relative IOD values were normalized to that of lane 1 and given below each blot. All experiments were repeated at least three times, and a representative result was shown.

Immunoprecipitation assay

HEK293T cells were transfected with the indicated plasmids using Lipofectamine 2000 according to the manufacturer's instructions. At 24 or 36 h posttransfection, the cells were lysed in immunoprecipitation lysis buffer (Beyotime, Jiangsu, China) with the addition of a protease inhibitor mixture (MCE) on ice. Subsequently, a portion of the cell lysate was used in the immunoprecipitation experiment by incubating it with anti-HA or anti-Flag magnetic beads at 4°C overnight while the remaining cell lysate was used as immunoprecipitation input. The endogenous immunoprecipitation was conducted using anti-DDX1, anti-DDX21, or anti-RTCB Abs with rabbit IgG Ab as a control. The cell lysate and Ab mixtures were incubated at 4°C overnight. On the next day, pretreated protein A/G agarose (Santa Cruz) was added to the mixtures and incubated at 4°C for another 2 h with rotation. The immunoprecipitated proteins and input cell lysates were analyzed by Western blotting as described earlier.

Luciferase reporter assay

HEK293T cells in 12-well plates were transfected with the internal control pRL-TK (10 ng/well) and IFN-β-luc, IFN-sensitive responsive element (ISRE)-luc, or NF-κB-luc (0.5 μg/well), along with siRTCB or an increasing amount of Myc-RTCB. To stimulate these promoters' luciferase activity, PR8 infection was conducted at 24 h posttransfection. At 24 h posttransfection or 12 hpi, cells were lysed in 200 μl of 1× passive lysis buffer (Promega). The luciferase activity and Renilla activity were measured using a dual-luciferase assay kit (Promega) according to the manufacturer's instructions. Renilla luciferase activity was used as an internal control to normalize transfection efficiency.

Determination of IFN concentration

Cell culture supernatants were centrifuged at 2300 × *g* for 5 min to eliminate cell debris. ELISA kits (Multi Sciences, Zhejiang, China) for human IFN-α, IFN-β, and IFN-λ were used to determine the concentration of the corresponding protein in cell culture supernatants. ELISA was performed according to the manufacturer's instructions.

Cell viability assay

Cell viability was assessed using a colorimetric-based cell counting kit-8 (CCK-8) assay (Dojindo Molecular Technologies). In brief, HEK293T cells in 96-well plates were transfected with siRTCB, siDDX1, or siNC, and cell viability was measured at 24 h posttransfection. We added 10 μl of CCK-8 reagent to each well of the plates, and cells were incubated at 37°C for 4 h. The absorbance of the reaction product in each well was measured using a microplate reader at 450 nm.

Statistical analysis

Data are expressed as the means ± SD of at least three independent experiments. Statistical analysis was performed by determining *p* values using the unpaired two-tailed Student *t* test or ANOVA (*$p < 0.05$, **$p < 0.01$, ***$p < 0.001$).

Results

RTCB expression is downregulated during IAV infection

RTCB has been shown to coimmunoprecipitate with IAV components in several studies, including ours (28–30). In addition, RNA sequencing data indicate that IAV infection leads to decreased RTCB expression in A549 cells (32). These results strongly suggest a potential role for RTCB in IAV infection. To determine whether RTCB downregulation is a consequence of IAV infection, we infected A549 cells with the H1N1-PR8 strain at an MOI of 0.5. At 12, 24, and 36 hpi, cells were harvested for reverse transcription-qPCR (RT-qPCR and Western blot assays. The results showed that both the mRNA and the protein levels of RTCB in PR8-infected cells were markedly reduced at all three time points (Fig. 1A–C). Accordingly, two additional IAV strains, H5 subtype (H5N6-JX) and H3 subtype (H3N2-HB), were evaluated to determine the potential regulation of RTCB expression. Similarly, we found that both H5N6-JX and H3N2-HB infections resulted in decreased mRNA abundance and protein yield of RTCB at 12, 24, and 36 hpi (Fig. 1D–I). Next, A549 cells were infected with PR8 at an MOI of 0.01, 0.1, and 1 for 24 hpi, and we assessed the mRNA and protein expression levels of RTCB. The results showed that RTCB mRNA and protein expression was downregulated in A549 cells during IAV infection in a dose-dependent manner (Fig. 1J–L).

We further determined whether virus-induced RTCB downregulation could be applied to other transformed cell types and human primary cells. Subsequently, we selected the THP1, U251, and HEK293T cell lines for evaluation because these three cell lines were susceptible to influenza infection, according to our pilot experiments (data not shown). THP1, U251, and HEK293T cells were infected with PR8 at MOI of 0.01, 0.1, and 1 for 24 hpi, followed by RTCB mRNA and protein measurements. This demonstrated that an increased PR8 viral challenge caused a gradient decrease in cellular RTCB expression in these three cell lines, as observed in A549 cells (Supplemental Fig. 1A–I). Importantly, we infected primary human type II alveolar epithelial cells with PR8 at an MOI of 0.1 for 24 hpi. Both RTCB mRNA and protein levels significantly decreased during IAV infection (Fig. 1M, 1N).

To determine the exact viral segment responsible for RTCB downregulation, we individually introduced eight viral proteins into A549 cells before assessing RTCB expression. Notably, no single PR8 gene segment was able to suppress RTCB expression, as seen during viral infection (Supplemental Fig. 1J, 1K), suggesting the involvement of a more complicated regulatory mechanism. To further examine whether the downregulation of RTCB was specific to IAV infection, we measured the expression level of RTCB in A549 cells treated with two other RNA viruses: VSV and SeV. We observed that RTCB mRNA and protein expression was markedly suppressed during VSV infection (Supplemental Fig. 1L–N). However, RTCB expression remained unaffected during SeV infection (Supplemental Fig. 1O–Q). Collectively, these data suggest that expression of the host factor RTCB can be disrupted and suppressed by influenza and other RNA viral infections, indicating a role for RTCB in infection events.

RTCB facilitates the propagation of IAV

To determine whether RTCB plays a role in IAV replication, we used CRISPR/Cas9 genome editing technology to explore whether RTCB loss affects influenza virus proliferation in A549, THP1, and U251 cell lines (31). Two sgRNAs targeting two different exons of the RTCB gene independently were designed, and both sgRNAs exhibited good performance in effectively diminishing RTCB protein expression compared with the sgRNA targeting the luciferase gene in A549 cells (Supplemental Fig. 2A). $RTCB^{KO}$ did not affect the viability of A549 cells (Supplemental Fig. 2B), confirming that the observed discrepancy in viral proliferation was not a result of defects in cell viability caused by the loss of RTCB. Next, we examined the influence of RTCB on IAV replication by determining the propagation kinetics of the PR8 virus in $RTCB^{KO}$ and $RTCB^{WT}$ A549 cells. The viral titer of the two $RTCB^{KO}$ lines was significantly lower than that of the WT cells at specific time points, consistent with the reduction in viral nucleoproteins (Fig. 2A, 2B). H5N6-JX and H3N2-HB were used to evaluate whether RTCB depletion exerted broad-spectrum antiviral

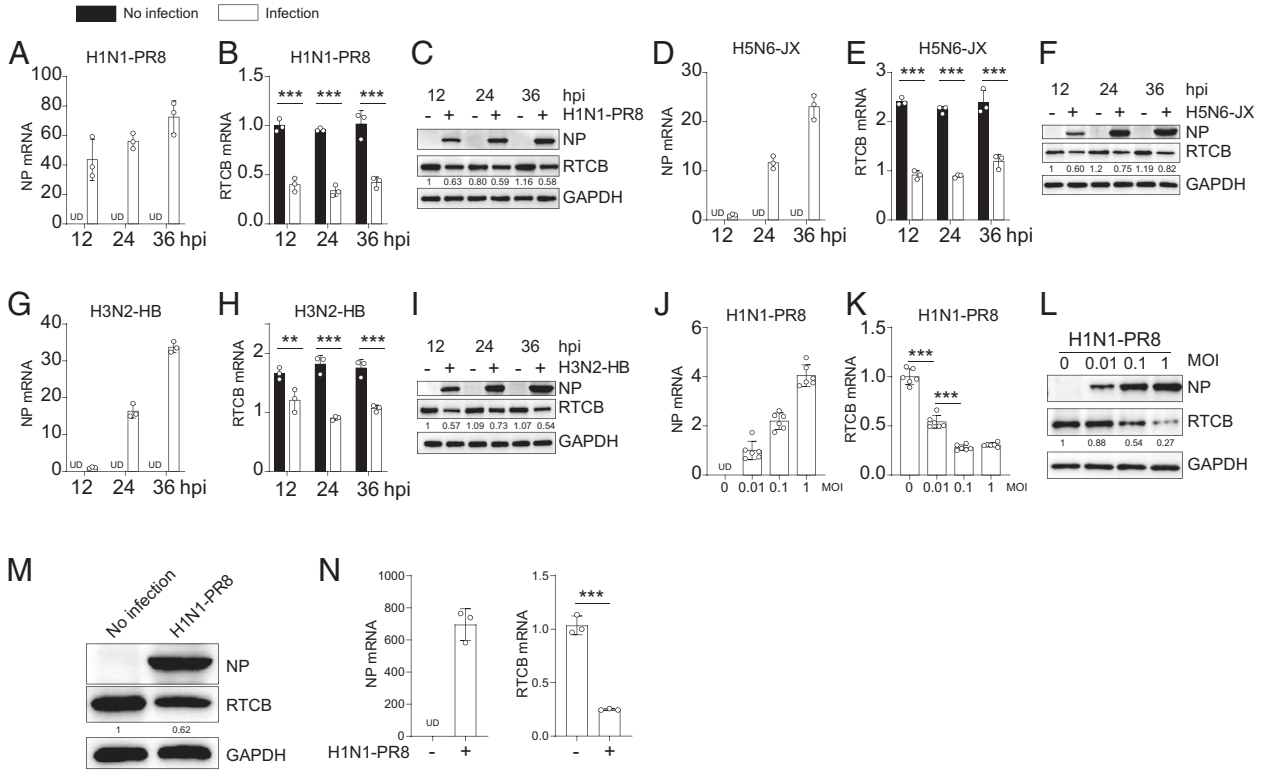

FIGURE 1. Cellular RTCB was downregulated in response to IAV infection. (**A–I**) A549 cells were infected with or without H1N1-PR8, H3N2-HB, or H5N6-JX virus at an MOI of 0.5. At 12, 24, and 36 hpi, the relative mRNA levels of RTCB and viral nucleoprotein were measured using qPCR, and the protein level was evaluated using Western blotting. (**J–L**) A549 cells were infected with the PR8 virus at the indicated doses for 24 h. The mRNA and protein levels of RTCB and viral nucleoproteins were detected using qPCR and Western blotting, respectively. (**M** and **N**) Primary human type II alveolar epithelial cells were infected with the PR8 virus (MOI = 0.1) for 24 h, the relative mRNA levels of RTCB and viral nucleoprotein were measured using qPCR, and the protein level was evaluated using Western blotting. GAPDH was used as the loading control for protein and mRNA expression normalization. In each Western blot assay, the blots originated either from the same membrane or from reloading the same quantity of lysates in the same experiments. Data were collected from three or six independent experiments as indicated and presented as the mean ± SD. Statistical significance was determined using the two-tailed Student *t* test (N), one-way ANOVA (K), and two-way ANOVA (B, E, and H). $^{**}p < 0.01$, $^{***}p < 0.001$. UD, undetermined.

activity against various subtypes of influenza viruses. As expected, RTCB-deficient A549 cells showed impaired H5N6-HB and H3N2-JX viral production, as measured using viral titers in the culture supernatants and viral nucleoprotein levels in the cell pellet (Fig. 2C–F). We also reduced the expression of RTCB in THP1, U251, and 293T cells using CRISPR genome editing or siRNA transfection to monitor the growth of the PR8 virus in these cells. This showed that the replication of PR8 was extensively hampered in RTCB-deficient cells (Fig. 2G–I). In parallel, we constructed a stable RTCB-overexpressing A549 cell line to perform the same assays (Supplemental Fig. 2C). As expected, the ectopic expression of RTCB favored the replication of PR8, as determined by the viral load and NP protein levels (Fig. 2J, 2K). This observation was reproduced in THP1, U351, and 293T cells (Supplemental Fig. 2D–F). Moreover, we infected $RTCB^{KO}$ and $RTCB^{WT}$ A549 cells with recombinant H5N6 or VSV-expressing GFP to evaluate the proviral effect of RTCB. $RTCB^{KO}$ significantly reduced the GFP signal of both viruses compared with that in $RTCB^{WT}$ A549 cells (Supplemental Fig. 2G, 2H). These results suggested that RTCB contributes to the proliferation of various subtypes of influenza viruses and other RNA viruses in A549 cells.

$RTCB^{KO}$ enhances IAV- or poly(IC)-triggered expression of IFNs

Because of the essential role of the RTCB in IAV replication, we explored the underlying mechanism. RTCB was initially identified through vRNP-associated coprecipitation; however, its involvement in the regulation of viral RNA synthesis remains unclear. Thus, a mini-replicon assay was used to evaluate the effect of RTCB on the polymerase activity of the PR8 H1N1 virus. RTCB overexpression had no obvious effect on polymerase activity (Supplemental Fig. 3A, 3B). Interestingly, previous studies have reported that RTCB is associated with DDX1, which has been shown to be an RNA sensor capable of activating innate immune responses (11). This prompted us to hypothesize that RTCB plays a role in antiviral immune response. To assess this, $RTCB^{KO}$ and $RTCB^{WT}$ A549 cells were infected with or without the PR8 virus for 12 and 24 h, followed by detecting the mRNA and protein levels of type I and III IFNs, including IFN-α, IFN-β, and IFN-λ. In uninfected A549 cells, RTCB depletion caused minimal changes in the mRNA and protein levels of these IFNs (Fig. 3A–C). However, upon viral stimulation, these antiviral cytokines sharply increased in level, and the loss of RTCB further elicited a favorable elevation in the levels of these IFNs compared with those in the control cells (Fig. 3A–C). Furthermore, we determined the expression levels of some IFN-? A3B2 tlsb -0.02w?>stimulated genes (ISGs), including IFIT2, ISG15, ISG56, IL-6, IL-8, and TNF-α, which were significantly higher in $RTCB^{KO}$ A549 cells than in control cells upon viral infection (Fig. 3D). Furthermore, we performed the same experiments in $RTCB^{KO}$ U251 and THP1 cells and found that the loss of RTCB clearly enhanced the cellular immune response during PR8 infection, similar to the measurement in $RTCB^{KO}$ A549 cells (Fig. 3E–H, Supplemental Fig. 3C–F). In the context of SeV infection, loss of RTCB also enhanced the expression of IFN-α in A549 cells (Supplemental Fig. 3G).

Poly(IC) is a synthetic analog of dsRNA that can trigger innate immune responses mediated by cytoplasmic pattern recognition receptors, including RIG-I, TLR3, MDA5, and DDX1 (11, 33). To

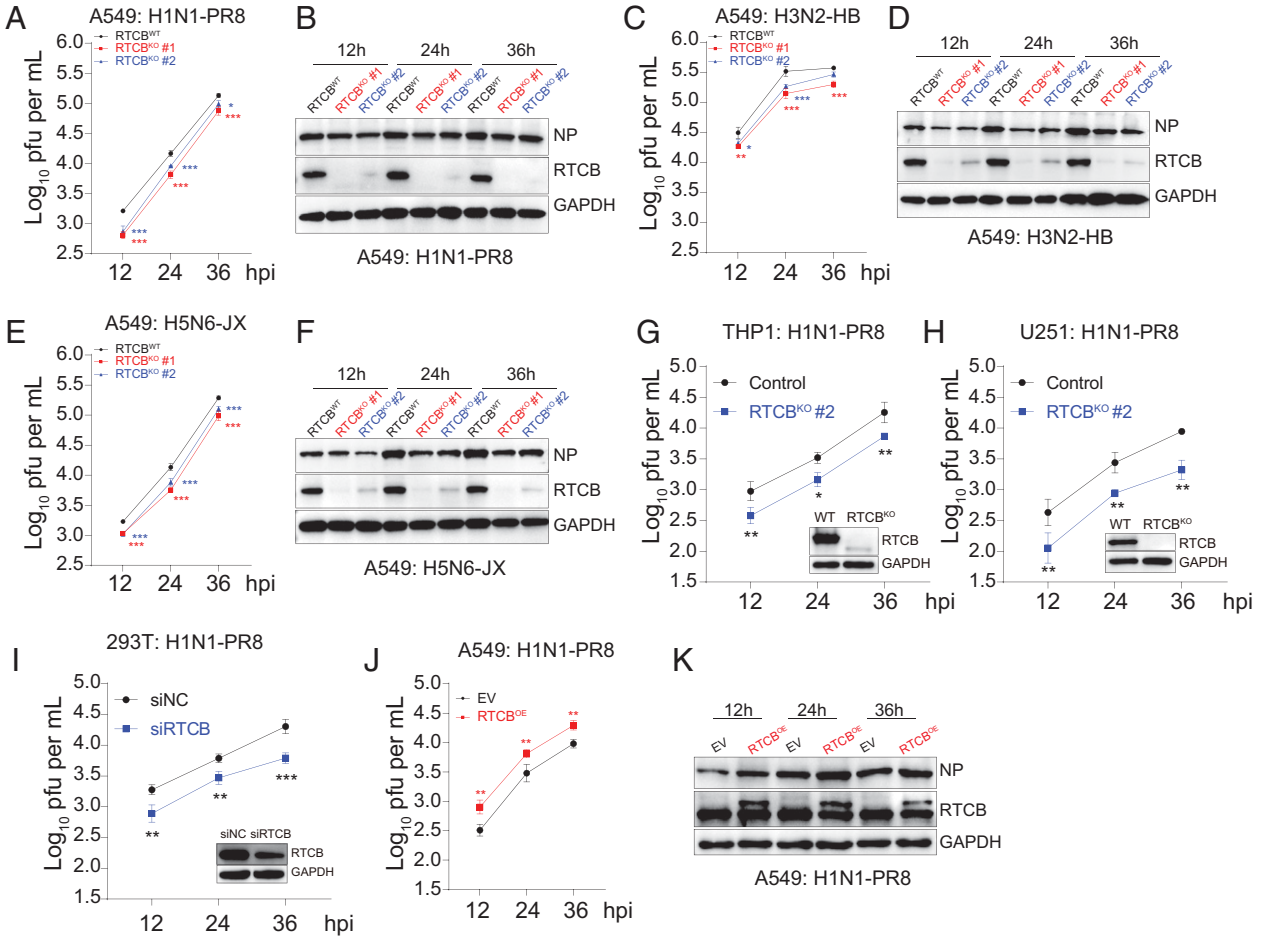

FIGURE 2. Loss of RTCB compromised IAV replication in A549 cells. (**A–F**) The effect of RTCB^{KO} on IAV replication. RTCB^{WT} and RTCB^{KO} A549 cells were infected with H1N1-PR8, H3N2-HB, or H5N6-JX viruses at an MOI of 0.01. The culture supernatants and the cell lysates were harvested at 12, 24, and 36 hpi. The virus titers were then determined using the plaque assay on MDCK cells, as shown in (A), (C), and (E). RTCB and viral nucleoproteins were probed using Western blotting, as shown in (B), (D), and (F). (**G** and **H**) RTCB^{KO} THP1 and U251 cells were infected with the PR8 virus (MOI = 0.01) for 12, 24, and 36 h, and the viral titers were determined using the plaque assay on MDCK cells. (**I**) HEK293T cells were transfected with RTCB or control siRNAs for 24 h, followed by infection with PR8 virus (MOI = 0.01). Cell supernatants were harvested at 12, 24, and 36 hpi. The virus titers were then determined using the plaque assay on MDCK cells. (**J** and **K**) The effect of overexpressed RTCB on IAV replication. RTCB-overexpressing A549 cells were infected with the H1N1-PR8 virus (MOI = 0.01). Cell supernatants and lysates were harvested at 12, 24, and 36 hpi for the plaque assay and Western blotting. In each Western blot assay, the blots originated either from the same membrane or from reloading the same quantity of lysates in the same experiments. Data were collected from three independent experiments and presented as the mean ± SD. Statistical significance was determined by two-way ANOVA. *$p < 0.05$, **$p < 0.01$, ***$p < 0.001$.

elucidate the action of RTCB after poly(IC)-triggered immune stimulation, we transfected the RTCB^{WT} or RTCB^{KO} A549 cells with 0.1 μM poly(IC) for 6 h, followed by the measurement of the levels of type I and III IFNs. We observed that poly(IC) induced a robust increase in IFN-α, IFN-β, and IFN-λ mRNA levels (Supplemental Fig. 3H). However, in the absence of RTCB, IFN-α, IFN-β, and IFN-λ reached notably higher levels than those observed in RTCB^{WT} cells (Supplemental Fig. 3H). Overall, our data suggest that endogenous RTCB negatively regulates IAV- and poly(IC)-triggered IFN expression, which is likely a mechanism harnessed by the host to defend against IAV infection (8).

RTCB suppresses IAV- or poly(IC)-triggered IFN expression

After revealing the important role of RTCB in IAV infection using loss-of-function assays, we aimed to confirm whether RTCB overexpression exerts the opposite effect on innate immune responses upon IAV stimulation. Therefore, we infected stably RTCB-overexpressing and WT A549 cells with PR8 for 12 and 24 h followed by IFN and cytokine detection. RTCB efficiently suppressed virus-induced IFN-α, IFN-β, and IFN-λ mRNA expression in A549 cells (Fig. 4A–C), and these findings were further corroborated by the detection of the protein levels of IFN-α, IFN-β, and IFN-λ in the supernatant (Fig. 4A–C). Concomitantly, the mRNA expression of a panel of ISGs that include IFIT2, ISG15, ISG56, IL-6, IL-8, and TNF-α also markedly declined with RTCB overexpression (Fig. 4D). These results were validated using U251 and THP1 cells stably overexpressing RTCB (Fig. 4E–H, Supplemental Fig. 4A–D). Similar results were observed in stably RTCB-overexpressing A549 cells transfected with poly(IC) (Supplemental Fig. 4E). Collectively, these data suggest that RTCB suppresses IAV- and poly(IC)-triggered immune responses.

RTCB inhibits the IAV-induced activation of IFN-β, ISRE, and NF-κB promoter activity

To further explore the role of RTCB in IAV-induced innate immune signaling pathways, we investigated the effect of RTCB on IAV-induced activation of the IFN-β promoter. HEK293T cells were cotransfected with IFN-β-Luc, pRL-TK, Myc-RTCB, or RTCB siRNAs. At 24 hpi, the cells were stimulated with PR8 for another 12 h, followed by a luciferase activity assay. The results showed that RTCB overexpression significantly reduced the IFN-β promoter activity in a dose-dependent

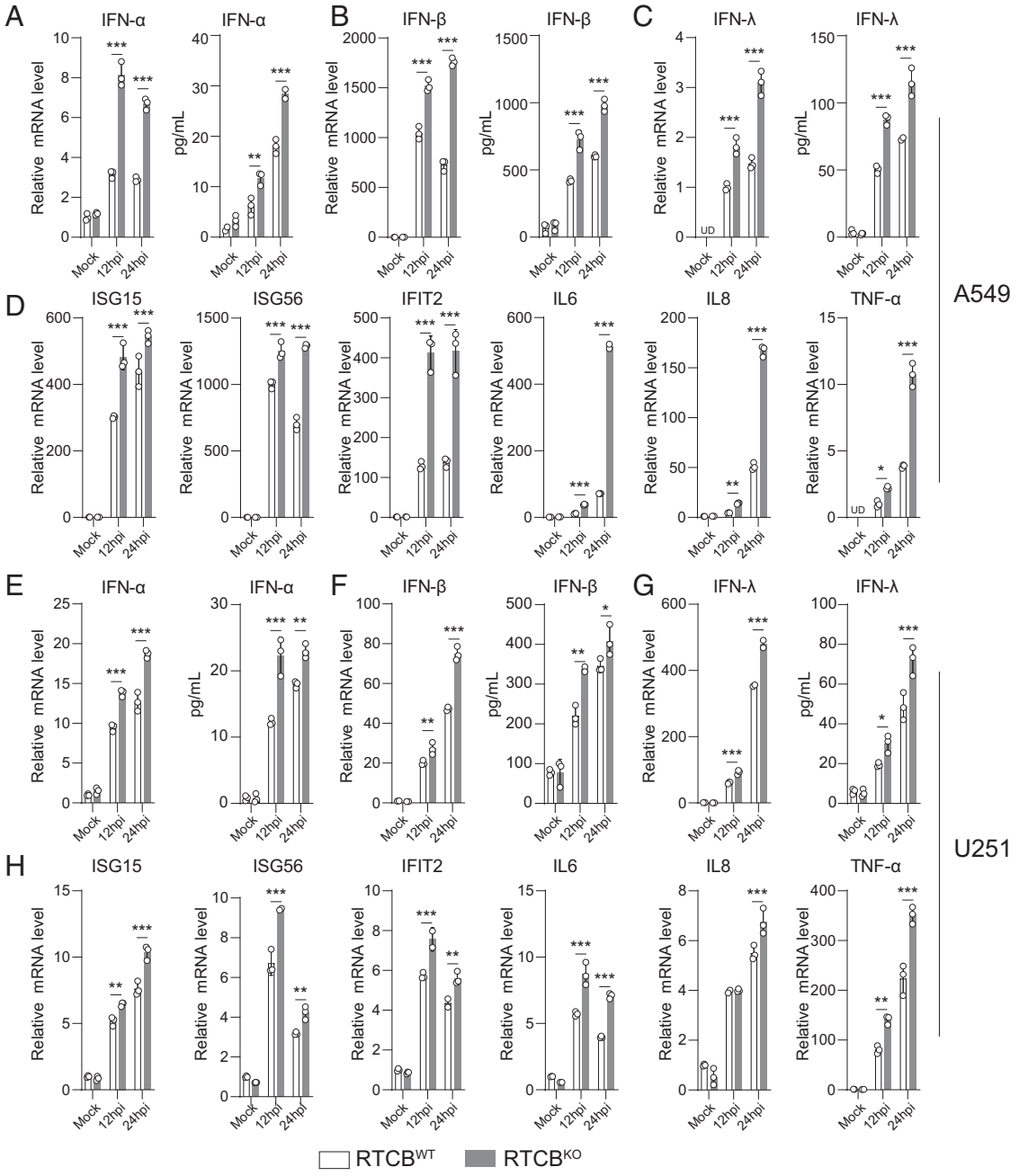

FIGURE 3. RTCB^{KO} enhanced IAV-induced IFN expression. (**A**–**C**) RTCB^{WT} and RTCB^{KO} A549 cells were mock infected or infected with PR8 (MOI = 0.1). At 12 and 24 hpi, the relative mRNA levels of IFN-α, IFN-β, and IFN-λ were measured using RT-qPCR, and the protein levels of IFN-α, IFN-β, and IFN-λ were determined using ELISA. (**D**) The relative mRNA levels of IL-6, IL-8, IFIT2, ISG15, ISG56, and TNF-α were measured using RT-qPCR. (**E**–**G**) RTCB^{WT} and RTCB^{KO} U251 cells were mock infected or infected with PR8 (MOI = 0.1). At 12 and 24 hpi, the relative mRNA levels of IFN-α, IFN-β, and IFN-λ were measured using RT-qPCR, and the protein levels of IFN-α, IFN-β, and IFN-λ were determined using ELISA. (**H**) The relative mRNA levels of IL-6, IL-8, IFIT2, ISG15, ISG56, and TNF-α in U251 cells were measured using RT-qPCR. Data were collected from three independent experiments as indicated and presented as the mean ± SD. Statistical significance was determined by two-way ANOVA. *$p < 0.05$, **$p < 0.01$, ***$p < 0.001$. UD, undetermined.

manner (Fig. 5A), whereas RTCB silencing enhanced the IFN-β promoter activity (Fig. 5D). It is thought that the expression of IFN-β is mainly regulated by the NF-κB and IFN regulatory factor (IRF) IRF3 (34, 35). To examine the effect of RTCB on IAV-induced activation of NF-κB and IRF3, we transfected the luciferase-expressing vector driven by either NF-κB or ISRE promoters in RTCB-overexpressing and RTCB-silenced HEK293T cells, followed by 12 h of PR8 stimulation. The results indicated that the promoter activity of NF-κB and ISRE declined with the increase of the RTCB expression level (Fig. 5B, 5C). Conversely, RTCB knockdown enhanced the luciferase activity of NF-κB and ISRE (Fig. 5E, 5F). Based on these observations, we investigated whether RTCB influences the protein levels of several key immune regulators upstream of IFN and cytokines, including MAVS, TBK1, IRF3, P65, and the phosphorylated versions of TBK1 (p-TBK1), IRF3 (p-IRF3), and P65 (p-P65). Therefore, we infected RTCB^{KO} and RTCB^{WT} A549 cells with PR8 at the indicated time points, and the protein levels of MAVS, TBK1, p-TBK1, IRF3, p-IRF3, P65, and p-P65 were determined using Western blotting. The data indicated that the phosphorylation of TBK1, IRF3, and P65 significantly

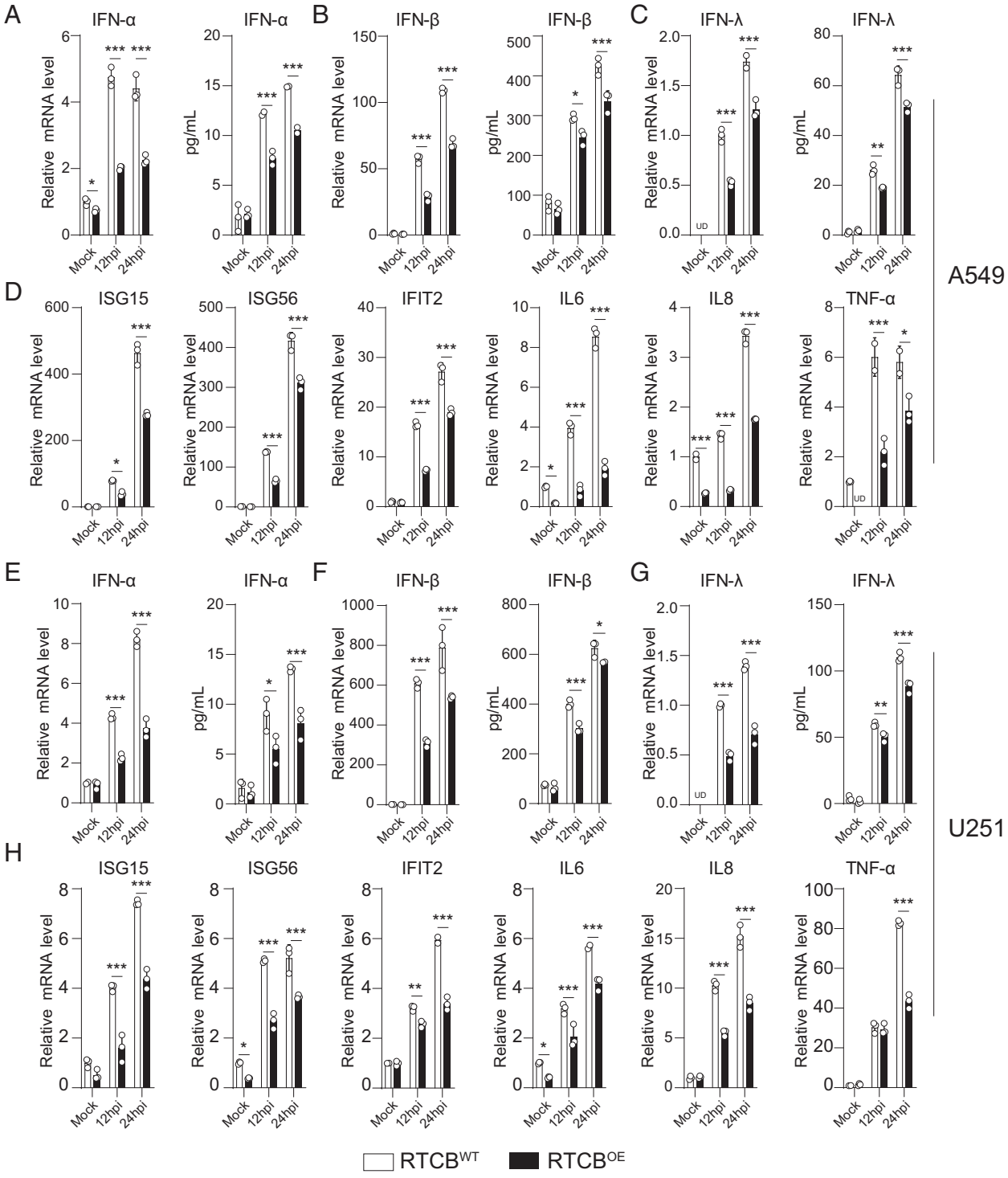

FIGURE 4. The induced expression of RTCB suppressed IFN production triggered by IAV infection. (**A**–**C**) RTCB-overexpressing A549 cells were infected with or without H1N1-PR8 (MOI = 0.1). At 12 and 24 hpi, the relative mRNA levels of IFN-α, IFN-β, and IFN-λ were determined using RT-qPCR, and the protein levels of IFN-α, IFN-β, and IFN-λ were measured using ELISA. (**D**) The mRNA abundance of IL-6, IL-8, IFIT2, ISG15, ISG56, and TNF-α was measured using RT-qPCR. (**E**–**G**) RTCB-overexpressing U251 cells were infected with or without H1N1-PR8 (MOI = 0.1). At 12 and 24 hpi, the relative mRNA levels of IFN-α, IFN-β, and IFN-λ were determined using RT-qPCR, and the protein levels of IFN-α, IFN-β, and IFN-λ were measured using ELISA. (**H**) The mRNA abundance of IL-6, IL-8, IFIT2, ISG15, ISG56, and TNF-α in U251 cells was measured using RT-qPCR. Data were collected from three independent experiments as indicated and presented as the mean ± SD. Statistical significance was determined by two-way ANOVA. $*p < 0.05$, $**p < 0.01$, $***p < 0.001$. UD, undetermined.

increased in RTCB-depleted cells compared with that in WT A549 cells, indicating a more activated antiviral response without RTCB (Fig. 5G). Collectively, these results suggest that RTCB inhibits the activation of antiviral signaling cascades induced by IAV infection.

RTCB affects IAV-induced IFN-β expression via interaction with DDX1

RTCB was reported to be associated with DDX1, which is a subunit of the tRNA ligase complex. Simultaneously, DDX1 also acts as an RNA sensor positively regulating the antiviral innate immunity of the human host. Our data in this study demonstrated that RTCB

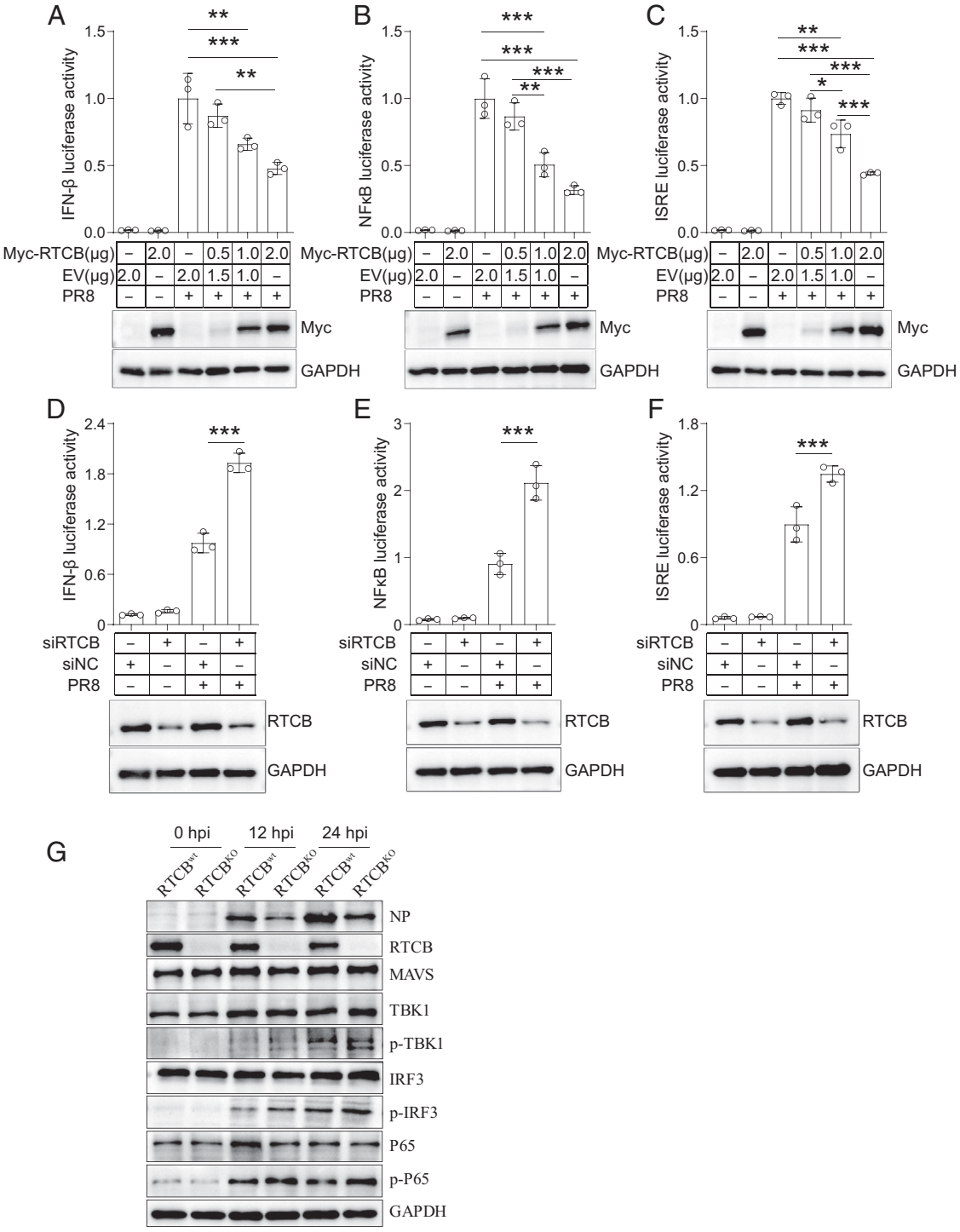

FIGURE 5. RTCB inhibited the IAV-induced activation of IFN-β, ISRE, and NF-κB promoter activity. (**A**–**C**) The effect of RTCB overexpression on IFN-β, ISRE, and NF-κB promoter activity. HEK293T cells were cotransfected with pRL-TK and increasing quantities of Myc-RTCB together with IFN-β-Luc (A), NF-κB-Luc (B), or ISRE-Luc (C). After 24 h, the cells were subjected to PR8 infection (MOI of 0.1). The luciferase activities were measured at 12 hpi, and *Renilla* luciferase was used as an internal control. The expression of RTCB was determined using Western blotting. (**D**–**F**) The effect of RTCB knockdown on IFN-β, ISRE, and NF-κB promoter activity. HEK293T cells were transfected with pRL-TK and siRTCB together with IFN-β-Luc (D), NF-κB-Luc (E), or ISRE-Luc (F) for 24 h, followed by PR8 infection. Luciferase activities were measured at 12 hpi, and *Renilla* luciferase was used as the internal control. (**G**) $RTCB^{WT}$ and $RTCB^{KO}$ A549 cells were infected with PR8 (MOI = 0.1). At 0, 12, and 24 hpi, the cells were lysed, and expression of the indicated proteins was measured using Western blotting. In each Western blot assay, the blots originated either from the same membrane or from reloading the same quantity of lysates in the same experiments. Data were collected from three independent experiments as indicated and presented as the mean ± SD. Statistical significance was determined by one-way ANOVA. $*p < 0.05$, $**p < 0.01$, $***p < 0.001$.

negatively regulates IAV- or poly(IC)-induced IFN-β production. The potential dual function of DDX1 led us to hypothesize that RTCB may participate in the DDX1-mediated antiviral immune responses. We first employed siRNAs to silence DDX1 expression in the A549 cells (Fig. 6A, 6B) without any obvious influence on the cell viability (Fig. 6C). We further analyzed the effect of DDX1 knockdown on IAV- and poly(IC)-induced IFN-β production. We found that both poly(IC) and PR8 infection sharply elevated IFN-β expression, and

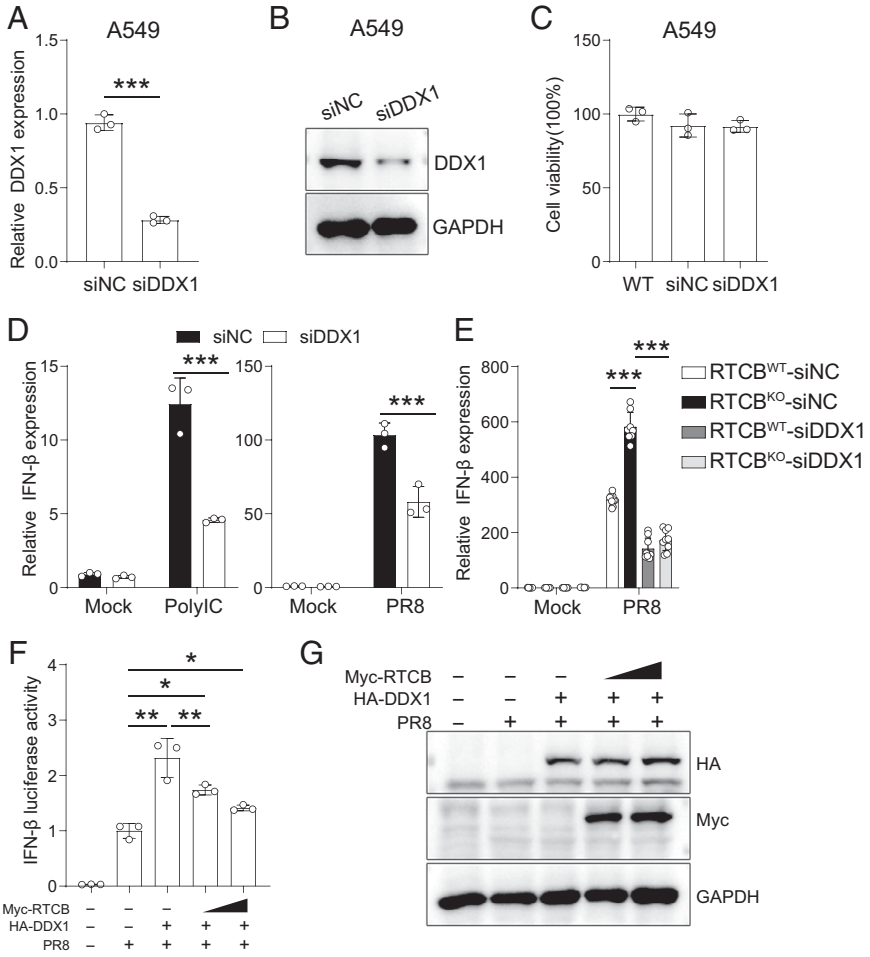

FIGURE 6. The inhibitory effect of RTCB on IFN-β expression is determined by DDX1 expression. (**A** and **B**) The knockdown efficiency of DDX1 was verified using qPCR and Western blotting. (**C**) Cell viability of A549 cells transfected with siDDX1 and control siNC was measured using the CCK-8 assay. (**D**) A549 cells were transfected with siNC or siDDX1 for 24 h, followed by treatment with poly(IC) (100 ng/ml) or by infection with PR8 (MOI = 0.1). After 12 h, the relative expression of IFN-β was measured using RT-qPCR. (**E**) $RTCB^{WT}$ and $RTCB^{KO}$ cells were transfected with siNC or siDDX1, followed by PR8 infection (MOI = 0.1). At 12 hpi, the relative expression of IFN-β was measured using RT-qPCR. (**F** and **G**) HEK293T cells were cotransfected with pRL-TK, HA-DDX1, IFN-β-Luc, and increasing amounts of Myc-RTCB, as indicated, for 24 h, followed by infection with PR8 (MOI = 0.1). Luciferase activities were measured using a luciferase report assay at 12 hpi, and *Renilla* luciferase was used as the internal control. The expression of RTCB and DDX1 was determined using Western blotting. In each Western blot assay, the blots originated either from the same membrane or from reloading the same quantity of lysates in the same experiments. Data were collected from three or nine independent experiments as indicated and presented as the mean ± SD. Statistical significance was determined using the two-tailed Student *t* test (A and D) or one-way ANOVA (E and F). $*p < 0.05$, $**p < 0.01$, $***p < 0.001$.

this increase in IFN-β expression was severely impaired after DDX1 knockdown (Fig. 6D). To better understand the interplay between RTCB and DDX1, we initially transfected the $RTCB^{WT}$ and $RTCB^{KO}$ A549 cells with either the scrambled siRNA or the siDDX1 before being infected with the PR8 virus. At 12 hpi, the mRNA level of IFN-β was measured. As expected, we found that the depletion of RTCB and DDX1 alone enhanced and attenuated the expression of virus-induced IFN-β, respectively. More importantly, when DDX1 was knocked down in $RTCB^{KO}$ cells, the level of IFN-β in these cells was comparable with that in $RTCB^{WT}$ cells (Fig. 6E), indicating that RTCB has lost its ability to regulate IFN-β expression in the absence of DDX1. In an IFN-β-luciferase assay, we showed that DDX1 increased the IFN-β promoter activity, which was attenuated by concurrent RTCB overexpression (Fig. 6F, 6G). Collectively, these data suggest that RTCB plays an important role in DDX1-mediated antiviral immune responses.

RTCB interacts with DDX1 and impedes its binding affinity to DDX21

Previously, RTCB was reported to be associated with DDX1 and to contribute to tRNA processing. Therefore, we hypothesized that the RTCB-DDX1 complex may play a role in modulating immune responses. To test this hypothesis, we analyzed the localization of RTCB and DDX1 by transfecting Myc-RTCB and HA-DDX1 into HeLa cells. As shown in Fig. 7A, RTCB colocalized with DDX1 in the cytosol. We performed coimmunoprecipitation (co-IP) to study the interactions between these two proteins. We demonstrated that RTCB can be immunoprecipitated using an anti-DDX1 Ab (Fig. 7B, left), and vice versa (Fig. 7B, right). A similar result was obtained when HA-tagged DDX1 and Myc-tagged RTCB were introduced into 293T cells for the co-IP assay (Fig. 7C). These results confirmed that RTCB binds to DDX1 in cells. DDX1 interacts directly with DDX21 in a complex of three dsRNA-sensing helicases (DDX1-DDX21-DHX36) that activate type I IFNs and cytokine responses (11, 12). Therefore, we speculated that the RTCB-DDX1 interaction may impair the DDX1-DDX21-DHX36 complex association, thereby suppressing type I IFNs and cytokine pathways. To test this hypothesis, we performed co-IP experiments on $RTCB^{WT}$ and $RTCB^{KO}$ A549 cells. Using DDX1 as bait, the amount of DDX21 immunoprecipitated by DDX1 was enhanced in $RTCB^{KO}$ cells (Fig. 7D), which could be reproduced by co-IP with an anti-DDX21 Ab (Fig. 7E). DHX36 could be immunoprecipitated by DDX21, but not by DDX1. In the plasmid transfection model using HA-DDX1 as bait, the amount of DDX21 immunoprecipitated with DDX1 gradually decreased with increasing RTCB expression (Fig. 7F). Concomitantly, a reduced amount of DDX1 that immunoprecipitated with DDX21 was observed with increased RTCB expression (Fig. 7G). The association between DHX36 and DDX21 was not disrupted by RTCB treatment (Fig. 7E, 7G). Based on these results, we proposed a model in which RTCB directly interacts with DDX1 and competitively inhibits the association of the DDX1-DDX21-DHX36 complex, thereby attenuating downstream signaling (Fig. 7H).

Discussion

In-depth functional and structural studies over a long period have demonstrated that RIG-I–like helicases selectively recognize viral RNA and trigger precise regulation of downstream signaling pathways (36).

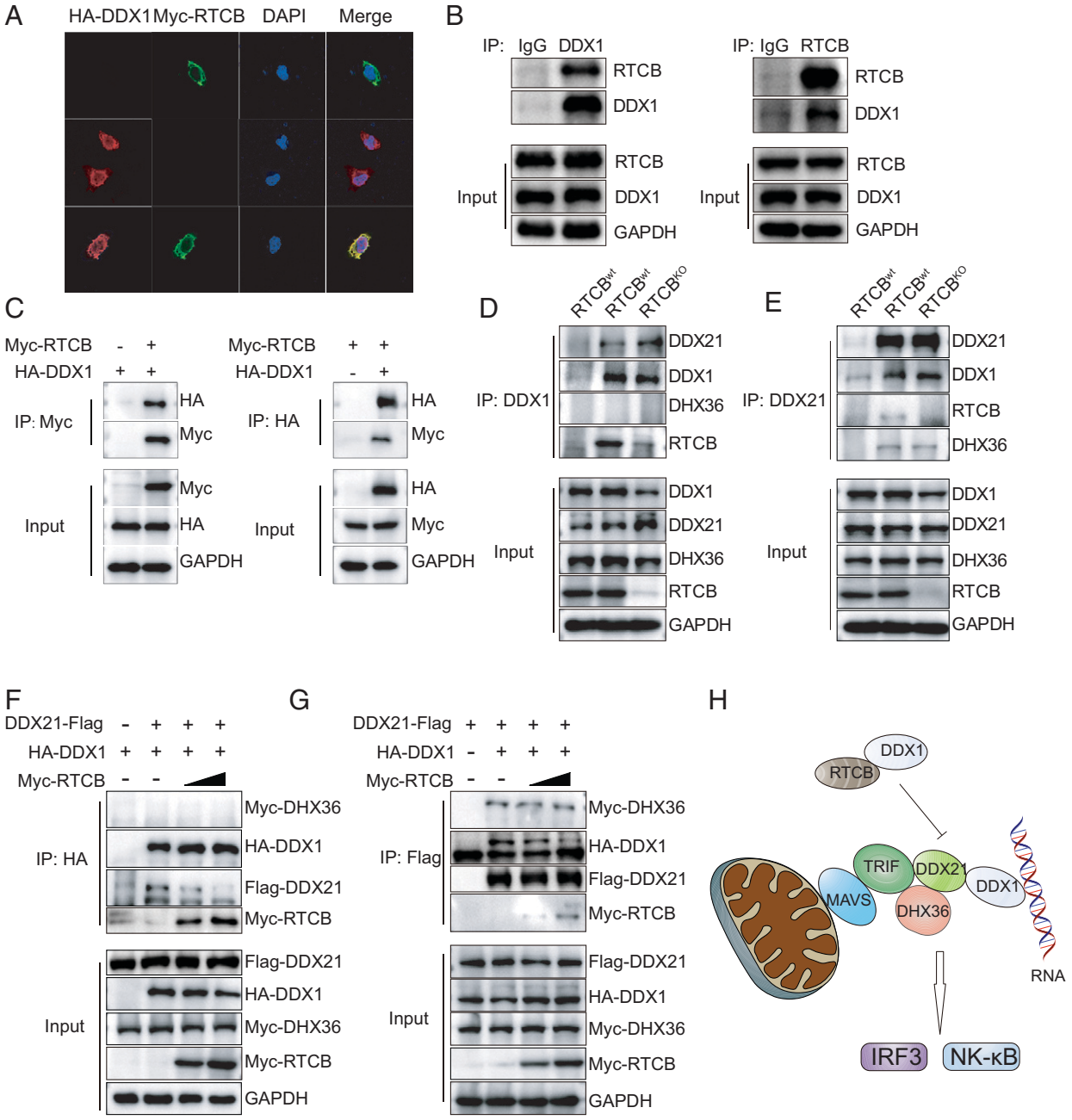

FIGURE 7. Protein–protein interaction between DDX1 and DDX21 was impeded by RTCB. (**A**) HeLa cells were cotransfected with Myc-RTCB and HA-DDX1. The localization of RTCB (green) and DDX1 (red) was assessed using confocal microscopy. DAPI was used to stain the nuclei (blue). (**B**) A549 cells from three 10-cm dishes were lysed with 500 μl IP lysis buffer, and immunoprecipitation was performed using anti-RTCB, anti-DDX1, or control IgG Abs. The pull-down products were analyzed using Western blotting. (**C**) HEK293T cells were cotransfected with Myc-RTCB and HA-DDX1. The co-IP experiment was performed using an anti-Myc or an anti-HA Ab, followed by Western blotting. (**D** and **E**) $RTCB^{WT}$ and $RTCB^{KO}$ A549 cells were cultured in 10-cm dishes and lysed with 500 μl IP lysis buffer, followed by immunoprecipitation assay with anti-DDX1, anti-DDX21, or control IgG; the pull-down products were analyzed using Western blotting. (**F** and **G**) HEK293T cells were cotransfected with HA-DDX1, Flag-DDX21, Myc-DHX36, or an empty vector, as well as with increasing quantities of Myc-RTCB for 24 h. The co-IP experiment was performed using an anti-HA or an anti-Flag Ab, followed by Western blotting. In each Western blot assay, the blots originated either from the same membrane or from reloading the same quantity of lysates in the same experiments. (**H**) The proposed model of the action of RTCB on the conformation of the DDX1-DDX21-DDX36 complex.

In particular, TRIM25-mediated RIG-I ubiquitination is critical for mitochondrial antiviral signaling protein binding and induction of antiviral signal transduction (37). In humans and other animals, the cellular helicase DDX1 plays an important role in recognizing dsRNAs and activating innate immune responses (11, 12, 38, 39). However, the precise regulatory mechanisms underlying DDX1-mediated antiviral innate immunity remain elusive. In this study, we demonstrated that RTCB negatively regulates DDX1-mediated anti-IAV innate immune responses by attenuating the binding affinity of DDX1 to DDX21, which facilitates the proliferation of the influenza virus.

In recent decades, mounting evidence from studies using various technologies, including RNA interference (40, 41), co-IP coupled to mass spectrometry (42), and CRISPR/Cas9 screening (43, 44) has revealed several novel proviral or antiviral factors that regulate IAV infection. These results are promising and provide valuable insights into the global understanding of IAV infection. Previously, our group,

in collaboration with others, identified the interaction between RTCB and viral RNP components; however, its role in the IAV life cycle has rarely been investigated (28, 30). In this study, we determined that RTCB expression was significantly reduced in A549 cells infected with H1N1, H3N2, and H5N6. This result was consistent with the findings of a previous study by Zhang et al. (32) in H3N2-infected A549 cells. Furthermore, a higher initial H1N1 virus challenge appeared to cause a greater decrease in RTCB expression in A549, THP1, U251, and HEK293T cells, indicating that this phenomenon may not be cell specific. Interestingly, we also discovered that RTCB expression was altered in A549 cells in response to IAV and VSV infections, but not to SeV infection, suggesting a special regulatory mechanism of RTCB by the two types of virus. Moreover, the downregulation of RTCB may be the result of the combined action of the influenza virus, because the eight viral gene segments were unable to decrease the level of RTCB expression individually. Importantly, we demonstrated that the expression of RTCB was also prominently decreased by influenza infection in primary human type II alveolar epithelial cells. Collectively, these results strongly suggest an important role for RTCB in influenza infection. However, the mechanism by which RTCB expression is downregulated during influenza infection remains unknown and requires further investigation.

Previous studies have shown that RTCB is involved in the life cycle of several other viruses, including hepatitis δ virus (26) and SINV (27), but the biological significance of altered RTCB expression remains unclear. We have demonstrated that the viral titers, as well as the viral protein yield, in the supernatants of PR8-infected $RTCB^{KO}$ or silenced cells (A549, THP1, U251, and HEK293T) were largely restricted, and this finding was validated using two other influenza viruses (HB and JX). Conversely, RTCB overexpression facilitated IAV replication, as determined by the viral titer and level of viral protein production. These results suggest a broad proviral spectrum of RTCB activity against the influenza virus. The activation of the innate immune response is an important strategy for the host to combat IAV infection in the early stages. To escape immune surveillance, the virus adopts immunomodulation strategies to antagonize the host IFN response and maintain its proliferation (45, 46). As a countermeasure, the expression of host factors is adjusted to enhance innate immune responses and protect against IAV infection (47). RTCB is a core component of the SF3b complex that participates in mRNA splicing and associates with the U2 small nuclear ribonucleoprotein (20), which is downregulated in response to IAV infection (32). In recent years, RTCB has been shown to interact with the influenza viral components NS1 and vRNP through several virus–host interactome screens (28–30); however, the biological implications of this molecular interplay during viral infection remain obscure. Initially, we hypothesized that RTCB–virus interactions may affect viral polymerase activity. However, based on our observations, RTCB did not affect viral polymerase activity, indicating a polymerase-independent mechanism of its antiviral role. Interestingly, $RTCB^{KO}$ enhanced the innate immune response in the context of IFNs or ISGs upon IAV infection or poly(IC) induction. This is attributed to the activation of immune pathways because we observed that the phosphorylation of TBK1, IRF3, and P65 was significantly increased in RTCB depletion cells in response to influenza virus infection, in accordance with the results of the IFN-β, NF-κB, and ISRE promoter activity test. We speculated that, besides its RNA splicing function, RTCB is most likely harnessed by the host to actively modulate immune response, which in turn helps to clear the viruses.

RTCB was previously determined to interact with DDX1, which is an important immune regulator in RNA sensing that forms a complex with DDX21 and DHX36 (11, 12, 20). In this study, we confirmed that RTCB colocalizes and interacts with DDX1 in A549 cells, consistent with previous findings (20). Furthermore, we showed that DDX1 silencing impairs the innate immune response to IAV infection. Importantly, in the absence of DDX1, $RTCB^{KO}$ lost its ability to promote an innate immune response. In addition, RTCB suppressed a DDX1-induced increase in IFN-β luciferase activity. These results indicate that RTCB-mediated immunosuppression is dependent on DDX1 expression. As previously reported, DDX1-mediated immune activation is largely attributable to the formation of the DDX1-DDX21-DDX36 complex, the disruption of which compromises the activation of downstream immune response signaling (13). DDX1 strongly pulled down both RTCB and DDX21 in the co-IP experiments. Notably, the association of DDX1 with DDX21 was severely impeded by an increase in RTCB expression, indicating dissociation of the DDX1-DDX21-DDX36 complex. We inferred that RTCB simultaneously participates in the formation of the tRNA ligase complex and the DDX1-DDX21-DHX36 complex, both of which direct two distinct biological processes. In the DExH/D-box helicases family, there are several other nucleic acid receptors, such as DDX3, DDX41, RIG-I, and DHX9 (48–50), among which RIG-I is critical for eliminating invaded viruses including influenza virus (17, 51, 52). These host factors have a synergistic effect on the regulation of viral replication. In fact, we investigated whether RTCB is involved in RIG-I–mediated immune responses. According to a co-IP experiment, we did not detect an interaction between RTCB and RIG-I (data not shown). This suggested that the modification of RTCB on immune response was not directly dependent on RIG-I. It reported that DHX36 was shown to interact with RIG-I in human and mouse cells (53), indicating a potential connection between the DDX1 and RIG-I pathways. It is possible that the cross-talk between DDX1 and RIG-I allowed a synergistic upregulation of IFNs by the release of RTCB from the DDX1-DDX21-DHX36 complex and the ensuing immune activation.

In summary, our results demonstrate that endogenous RTCB was downregulated in response to IAV infection, indicating that RTCB inhibition contributes to the restriction of IAV replication. We further showed that RTCB negatively regulated IAV-induced antiviral innate immune responses by impeding the binding of DDX1 to DDX21, thereby suppressing the expression of IFN and proinflammatory cytokines. Our study improves our understanding of RTCB as an immunomodulator and broadens its application as a therapeutic target for controlling viral infections.

Acknowledgments

We thank Hualan Chen (Harbin Veterinary Research Institute) for providing the VSV-GFP virus and Zhengfan Jiang (Peking University) for the luciferase reporter constructs and SeV.

Disclosures

The authors have no financial conflicts of interest.

References

1. Moeller, A., R. N. Kirchdoerfer, C. S. Potter, B. Carragher, and I. A. Wilson. 2012. Organization of the influenza virus replication machinery. *Science* 338: 1631–1634.
2. Molinari, N. A., I. R. Ortega-Sanchez, M. L. Messonnier, W. W. Thompson, P. M. Wortley, E. Weintraub, and C. B. Bridges. 2007. The annual impact of seasonal influenza in the US: measuring disease burden and costs. *Vaccine* 25: 5086–5096.
3. Zheng, W., and Y. J. Tao. 2013. Structure and assembly of the influenza A virus ribonucleoprotein complex. *FEBS Lett.* 587: 1206–1214.
4. Wu, W., and J. P. Metcalf. 2020. The role of type I IFNs in influenza: antiviral superheroes or immunopathogenic villains? *J. Innate Immun.* 12: 437–447.
5. Chen, X., S. Liu, M. U. Goraya, M. Maarouf, S. Huang, and J. L. Chen. 2018. Host immune response to influenza A virus infection. *Front. Immunol.* 9: 320.
6. Tisoncik, J. R., M. J. Korth, C. P. Simmons, J. Farrar, T. R. Martin, and M. G. Katze. 2012. Into the eye of the cytokine storm. *Microbiol. Mol. Biol. Rev.* 76: 16–32.
7. Liu, Q., Y. H. Zhou, and Z. Q. Yang. 2016. The cytokine storm of severe influenza and development of immunomodulatory therapy. *Cell. Mol. Immunol.* 13: 3–10.

8. Durbin, J. E., A. Fernandez-Sesma, C. K. Lee, T. D. Rao, A. B. Frey, T. M. Moran, S. Vukmanovic, A. García-Sastre, and D. E. Levy. 2000. Type I IFN modulates innate and specific antiviral immunity. *J. Immunol.* 164: 4220–4228.
9. McNab, F., K. Mayer-Barber, A. Sher, A. Wack, and A. O'Garra. 2015. Type I interferons in infectious disease. *Nat. Rev. Immunol.* 15: 87–103.
10. Takeuchi, O., and S. Akira. 2010. Pattern recognition receptors and inflammation. *Cell* 140: 805–820.
11. Zhang, Z., T. Kim, M. Bao, V. Facchinetti, S. Y. Jung, A. A. Ghaffari, J. Qin, G. Cheng, and Y. J. Liu. 2011. DDX1, DDX21, and DHX36 helicases form a complex with the adaptor molecule TRIF to sense dsRNA in dendritic cells. *Immunity* 34: 866–878.
12. Gantier, M. P., and B. R. Williams. 2011. Making sense of viral RNA sensing. *Mol. Ther.* 19: 1578–1581.
13. Wu, W., Y. Qu, S. Yu, S. Wang, Y. Yin, Q. Liu, C. Meng, Y. Liao, Z. Ur Rehman, L. Tan, et al. 2021. Caspase-dependent cleavage of DDX21 suppresses host innate immunity. *MBio* 12: e0100521.
14. Takeuchi, O., and S. Akira. 2007. Recognition of viruses by innate immunity. *Immunol. Rev.* 220: 214–224.
15. Muñoz-Moreno, R., C. Martínez-Romero, and A. García-Sastre. 2021. Induction and evasion of type-I interferon responses during influenza A virus infection. *Cold Spring Harb. Perspect. Med.* 11: a038414.
16. Gack, M. U., R. A. Albrecht, T. Urano, K. S. Inn, I. C. Huang, E. Carnero, M. Farzan, S. Inoue, J. U. Jung, and A. García-Sastre. 2009. Influenza A virus NS1 targets the ubiquitin ligase TRIM25 to evade recognition by the host viral RNA sensor RIG-I. *Cell Host Microbe* 5: 439–449.
17. Iwasaki, A., and P. S. Pillai. 2014. Innate immunity to influenza virus infection. *Nat. Rev. Immunol.* 14: 315–328.
18. Wang, R., Y. Zhu, X. Lin, C. Ren, J. Zhao, F. Wang, X. Gao, R. Xiao, L. Zhao, H. Chen, et al. 2019. Influenza M2 protein regulates MAVS-mediated signaling pathway through interacting with MAVS and increasing ROS production. *Autophagy* 15: 1163–1181.
19. Chen, G., C. H. Liu, L. Zhou, and R. M. Krug. 2014. Cellular DDX21 RNA helicase inhibits influenza A virus replication but is counteracted by the viral NS1 protein. *Cell Host Microbe* 15: 484–493.
20. Popow, J., M. Englert, S. Weitzer, A. Schleiffer, B. Mierzwa, K. Mechtler, S. Trowitzsch, C. L. Will, R. Lührmann, D. Söll, and J. Martinez. 2011. HSPC117 is the essential subunit of a human tRNA splicing ligase complex. *Science* 331: 760–764.
21. Popow, J., J. Jurkin, A. Schleiffer, and J. Martinez. 2014. Analysis of orthologous groups reveals archease and DDX1 as tRNA splicing factors. *Nature* 511: 104–107.
22. Chan, C. M., C. Zhou, and R. H. Huang. 2009. Reconstituting bacterial RNA repair and modification in vitro. *Science* 326: 247.
23. Litke, J. L., and S. R. Jaffrey. 2019. Highly efficient expression of circular RNA aptamers in cells using autocatalytic transcripts. *Nat. Biotechnol.* 37: 667–675.
24. Jurkin, J., T. Henkel, A. F. Nielsen, M. Minnich, J. Popow, T. Kaufmann, K. Heindl, T. Hoffmann, M. Busslinger, and J. Martinez. 2014. The mammalian tRNA ligase complex mediates splicing of XBP1 mRNA and controls antibody secretion in plasma cells. *EMBO J.* 33: 2922–2936.
25. Ray, A., S. Zhang, C. Rentas, K. A. Caldwell, and G. A. Caldwell. 2014. RTCB-1 mediates neuroprotection via XBP-1 mRNA splicing in the unfolded protein response pathway. *J. Neurosci.* 34: 16076–16085.
26. Cao, D., D. Haussecker, Y. Huang, and M. A. Kay. 2009. Combined proteomic-RNAi screen for host factors involved in human hepatitis delta virus replication. *RNA* 15: 1971–1979.
27. Garcia-Moreno, M., M. Noerenberg, S. Ni, A. I. Järvelin, E. González-Almela, C. E. Lenz, M. Bach-Pages, V. Cox, R. Avolio, T. Davis, et al. 2019. System-wide profiling of RNA-binding proteins uncovers key regulators of virus infection. *Mol. Cell* 74: 196–211.e11.
28. Yang, C., X. Liu, Q. Gao, T. Cheng, R. Xiao, F. Ming, S. Zhang, M. Jin, H. Chen, W. Ma, and H. Zhou. 2018. The nucleolar protein LYAR facilitates ribonucleoprotein assembly of influenza A virus. *J. Virol.* 92: e01042-18.
29. Watanabe, T., E. Kawakami, J. E. Shoemaker, T. J. Lopes, Y. Matsuoka, Y. Tomita, H. Kozuka-Hata, T. Gorai, T. Kuwahara, E. Takeda, et al. 2014. Influenza virus-host interactome screen as a platform for antiviral drug development. *Cell Host Microbe* 16: 795–805.
30. Wang, L., B. Fu, W. Li, G. Patil, L. Liu, M. E. Dorf, and S. Li. 2017. Comparative influenza protein interactomes identify the role of plakophilin 2 in virus restriction. *Nat. Commun.* 8: 13876.
31. Sander, J. D., and J. K. Joung. 2014. CRISPR-Cas systems for editing, regulating and targeting genomes. *Nat. Biotechnol.* 32: 347–355.
32. Zhang, Y., T. Yu, Y. Ding, Y. Li, J. Lei, B. Hu, and J. Zhou. 2020. Analysis of expression profiles of long noncoding RNAs and mRNAs in A549 cells infected with H3N2 swine influenza virus by RNA sequencing. *Virol. Sin.* 35: 171–180.
33. Gitlin, L., W. Barchet, S. Gilfillan, M. Cella, B. Beutler, R. A. Flavell, M. S. Diamond, and M. Colonna. 2006. Essential role of mda-5 in type I IFN responses to polyriboinosinic:polyribocytidylic acid and encephalomyocarditis picornavirus. *Proc. Natl. Acad. Sci. USA* 103: 8459–8464.
34. Tailor, P., T. Tamura, and K. Ozato. 2006. IRF family proteins and type I interferon induction in dendritic cells. *Cell Res.* 16: 134–140.
35. Pfeffer, L. M. 2011. The role of nuclear factor κB in the interferon response. *J. Interferon Cytokine Res.* 31: 553–559.
36. Yoneyama, M., K. Onomoto, M. Jogi, T. Akaboshi, and T. Fujita. 2015. Viral RNA detection by RIG-I-like receptors. *Curr. Opin. Immunol.* 32: 48–53.
37. Gack, M. U., Y. C. Shin, C. H. Joo, T. Urano, C. Liang, L. Sun, O. Takeuchi, S. Akira, Z. Chen, S. Inoue, and J. U. Jung. 2007. TRIM25 RING-finger E3 ubiquitin ligase is essential for RIG-I-mediated antiviral activity. *Nature* 446: 916–920.
38. Zhang, H., X. Song, T. Li, J. Wang, B. Xing, X. Zhai, J. Luo, X. Hu, X. Hou, and L. Wei. 2021. DDX1 from Cherry valley duck mediates signaling pathways and anti-NDRV activity. *Vet. Res. (Faisalabad)* 52: 9.
39. Lin, Z., J. Wang, W. Zhu, X. Yu, Z. Wang, J. Ma, H. Wang, Y. Yan, J. Sun, and Y. Cheng. 2021. Chicken DDX1 acts as an RNA sensor to mediate IFN-β signaling pathway activation in antiviral innate immunity. *Front. Immunol.* 12: 742074.
40. Karlas, A., N. Machuy, Y. Shin, K. P. Pleissner, A. Artarini, D. Heuer, D. Becker, H. Khalil, L. A. Ogilvie, S. Hess, et al. 2010. Genome-wide RNAi screen identifies human host factors crucial for influenza virus replication. *Nature* 463: 818–822.
41. Su, W. C., Y. C. Chen, C. H. Tseng, P. W. Hsu, K. F. Tung, K. S. Jeng, and M. M. Lai. 2013. Pooled RNAi screen identifies ubiquitin ligase Itch as crucial for influenza A virus release from the endosome during virus entry. *Proc. Natl. Acad. Sci. USA* 110: 17516–17521.
42. Heaton, N. S., N. Moshkina, R. Fenouil, T. J. Gardner, S. Aguirre, P. S. Shah, N. Zhao, L. Manganaro, J. F. Hultquist, J. Noel, et al. 2016. Targeting viral proteostasis limits influenza virus, HIV, and dengue virus infection. [Published erratum appears in 2016 *Immunity* 44: 438.] *Immunity* 44: 46–58 .
43. Han, J., J. T. Perez, C. Chen, Y. Li, A. Benitez, M. Kandasamy, Y. Lee, J. Andrade, B. tenOever, and B. Manicassamy. 2018. Genome-wide CRISPR/Cas9 screen identifies host factors essential for influenza virus replication. *Cell Rep.* 23: 596–607.
44. Li, B., S. M. Clohisey, B. S. Chia, B. Wang, A. Cui, T. Eisenhaure, L. D. Schweitzer, P. Hoover, N. J. Parkinson, A. Nachshon, et al. 2020. Genome-wide CRISPR screen identifies host dependency factors for influenza A virus infection. *Nat. Commun.* 11: 164.
45. Varga, Z. T., I. Ramos, R. Hai, M. Schmolke, A. García-Sastre, A. Fernandez-Sesma, and P. Palese. 2011. The influenza virus protein PB1-F2 inhibits the induction of type I interferon at the level of the MAVS adaptor protein. *PLoS Pathog.* 7: e1002067.
46. Lamotte, L. A., and L. Tafforeau. 2021. How influenza A virus NS1 deals with the ubiquitin system to evade innate immunity. *Viruses* 13: 2309.
47. Yang, C., X. Liu, T. Cheng, R. Xiao, Q. Gao, F. Ming, M. Jin, H. Chen, and H. Zhou. 2019. LYAR suppresses beta interferon induction by targeting phosphorylated interferon regulatory factor 3. *J. Virol.* 93: e00769-19.
48. Oshiumi, H., K. Sakai, M. Matsumoto, and T. Seya. 2010. DEAD/H BOX 3 (DDX3) helicase binds the RIG-I adaptor IPS-1 to up-regulate IFN-beta-inducing potential. *Eur. J. Immunol.* 40: 940–948.
49. Kim, T., S. Pazhoor, M. Bao, Z. Zhang, S. Hanabuchi, V. Facchinetti, L. Bover, J. Plumas, L. Chaperot, J. Qin, and Y. J. Liu. 2010. Aspartate-glutamate-alanine-histidine box motif (DEAH)/RNA helicase A helicases sense microbial DNA in human plasmacytoid dendritic cells. *Proc. Natl. Acad. Sci. USA* 107: 15181–15186.
50. Zhang, Z., B. Yuan, M. Bao, N. Lu, T. Kim, and Y. J. Liu. 2011. The helicase DDX41 senses intracellular DNA mediated by the adaptor STING in dendritic cells. [Published erratum appears in 2012 *Nat. Immunol.* 13: 196.] *Nat. Immunol.* 12: 959–965.
51. Kato, H., O. Takeuchi, S. Sato, M. Yoneyama, M. Yamamoto, K. Matsui, S. Uematsu, A. Jung, T. Kawai, K. J. Ishii, et al. 2006. Differential roles of MDA5 and RIG-I helicases in the recognition of RNA viruses. *Nature* 441: 101–105.
52. Kato, H., S. Sato, M. Yoneyama, M. Yamamoto, S. Uematsu, K. Matsui, T. Tsujimura, K. Takeda, T. Fujita, O. Takeuchi, and S. Akira. 2005. Cell type-specific involvement of RIG-I in antiviral response. *Immunity* 23: 19–28.
53. Yoo, J. S., K. Takahasi, C. S. Ng, R. Ouda, K. Onomoto, M. Yoneyama, J. C. Lai, S. Lattmann, Y. Nagamine, T. Matsui, et al. 2014. DHX36 enhances RIG-I signaling by facilitating PKR-mediated antiviral stress granule formation. *PLoS Pathog.* 10: e1004012.